Electronic Supplementary information (ESI) for

1,8-Naphthyridine-based fluorescent receptors for picric acid detection in aqueous media

Mandeep K. Chahal and Muniappan Sankar*

Department of Chemistry, Indian Institute of Technology Roorkee, Roorkee – 247667, India

E-mail: sankafcy@iitr.ac.in

Table of Contents

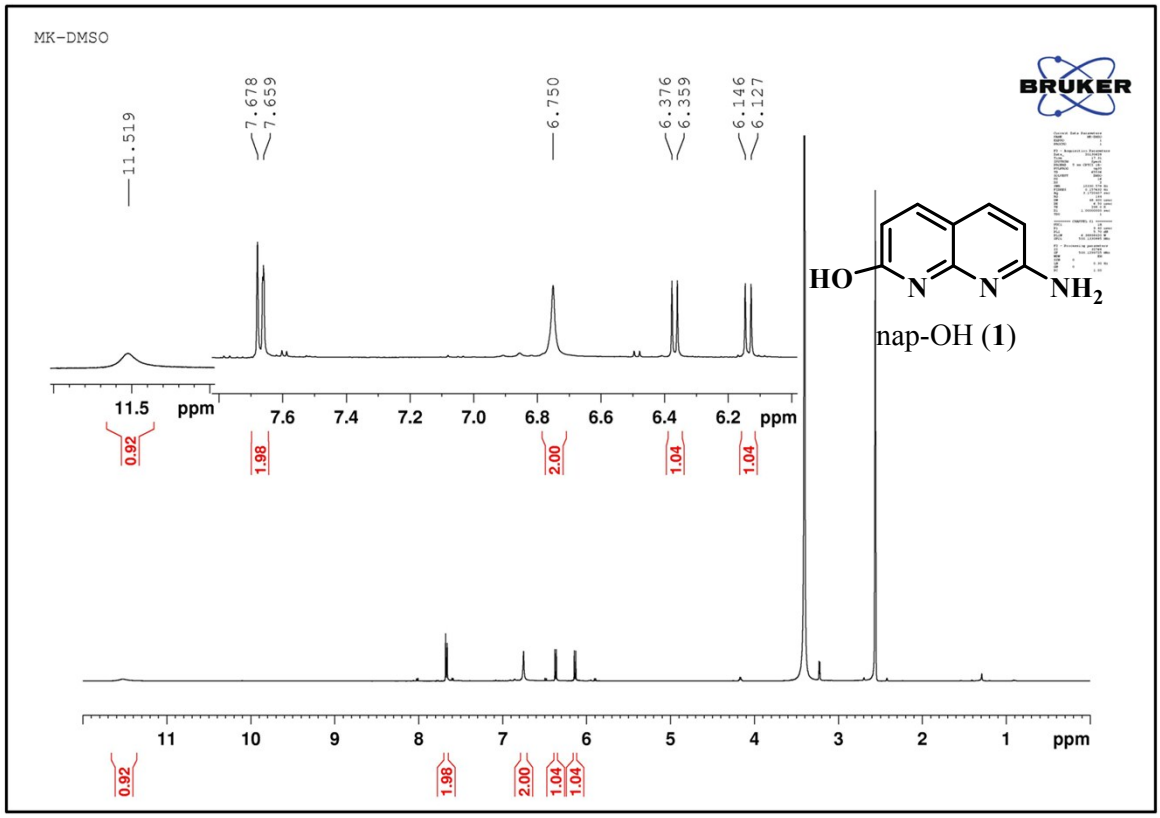

Figure S1. ^{1}H NMR spectrum of **1** in DMSO-d_6 at 298 K.

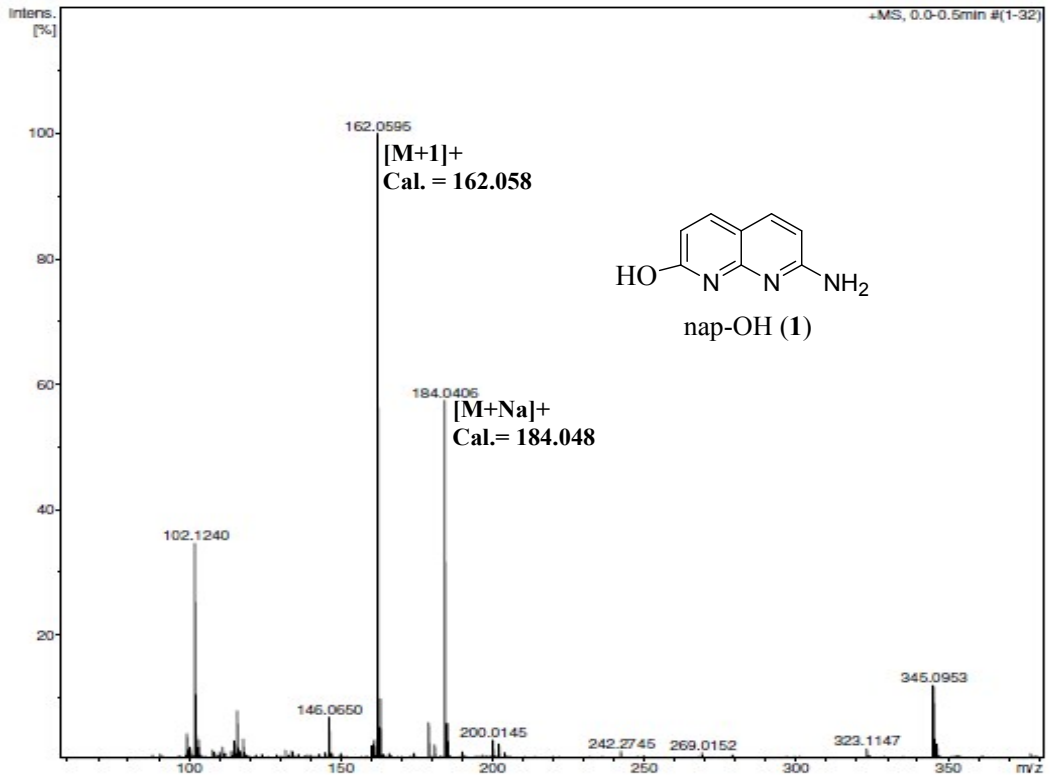

Figure S2. HRMS (ESI+) spectrum of **1** in CH_3CN.

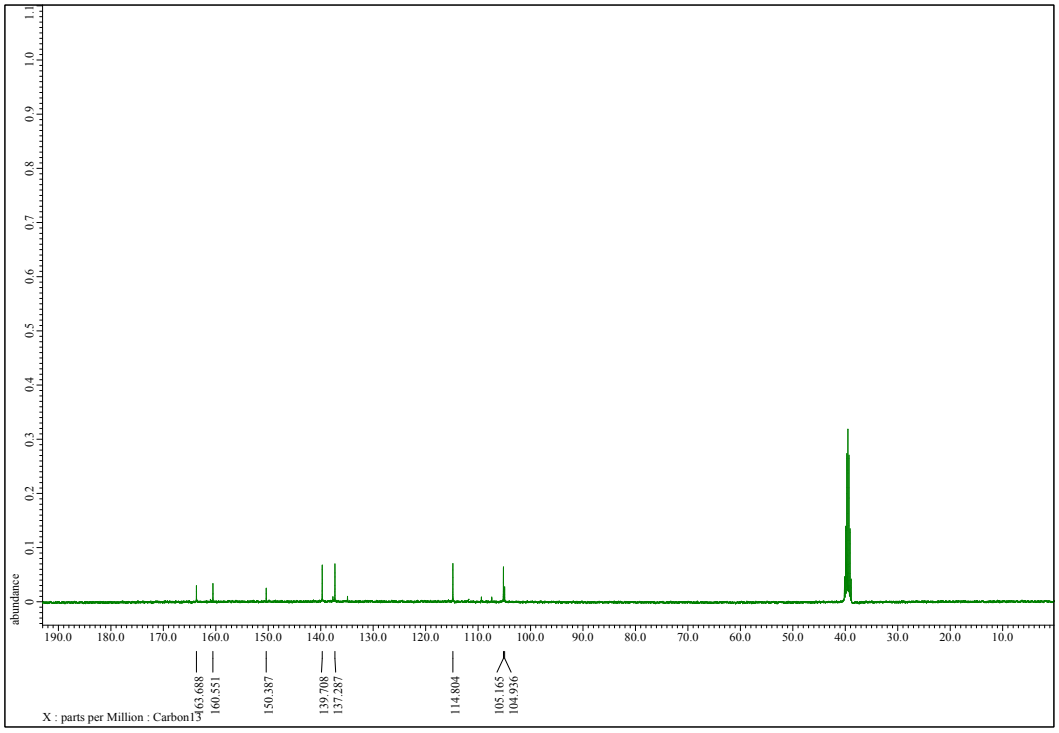

Figure S3. ^{13}C NMR spectrum of **1** in DMSO-d_6.

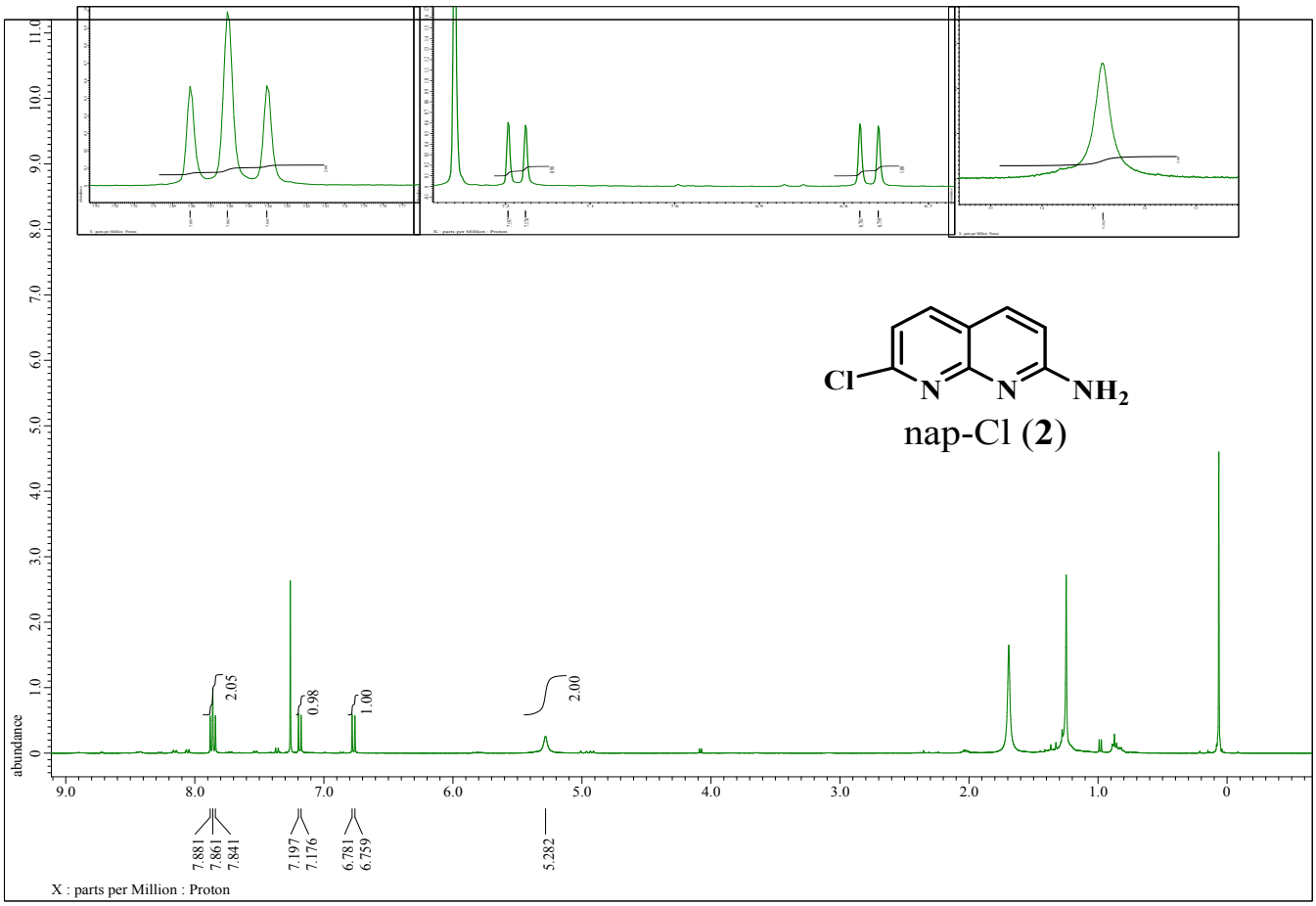

Figure S4. ^{1}H NMR spectrum of **2** in $CDCl_3$.

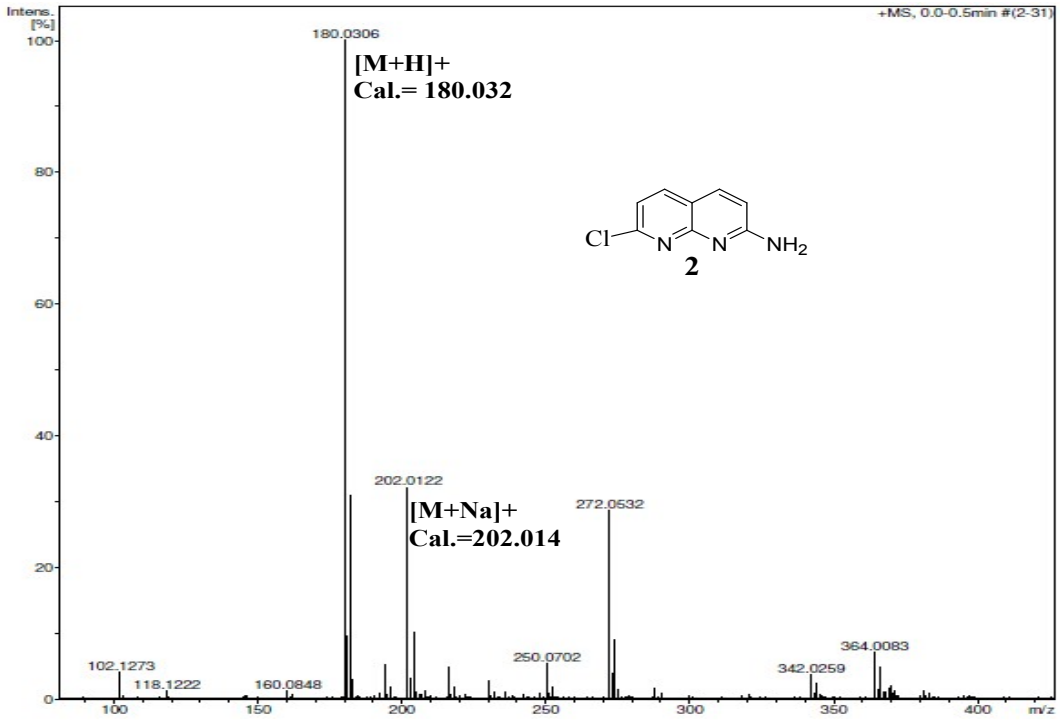

Figure S5. HRMS (ESI+) spectrum of **2** in CH_3CN.

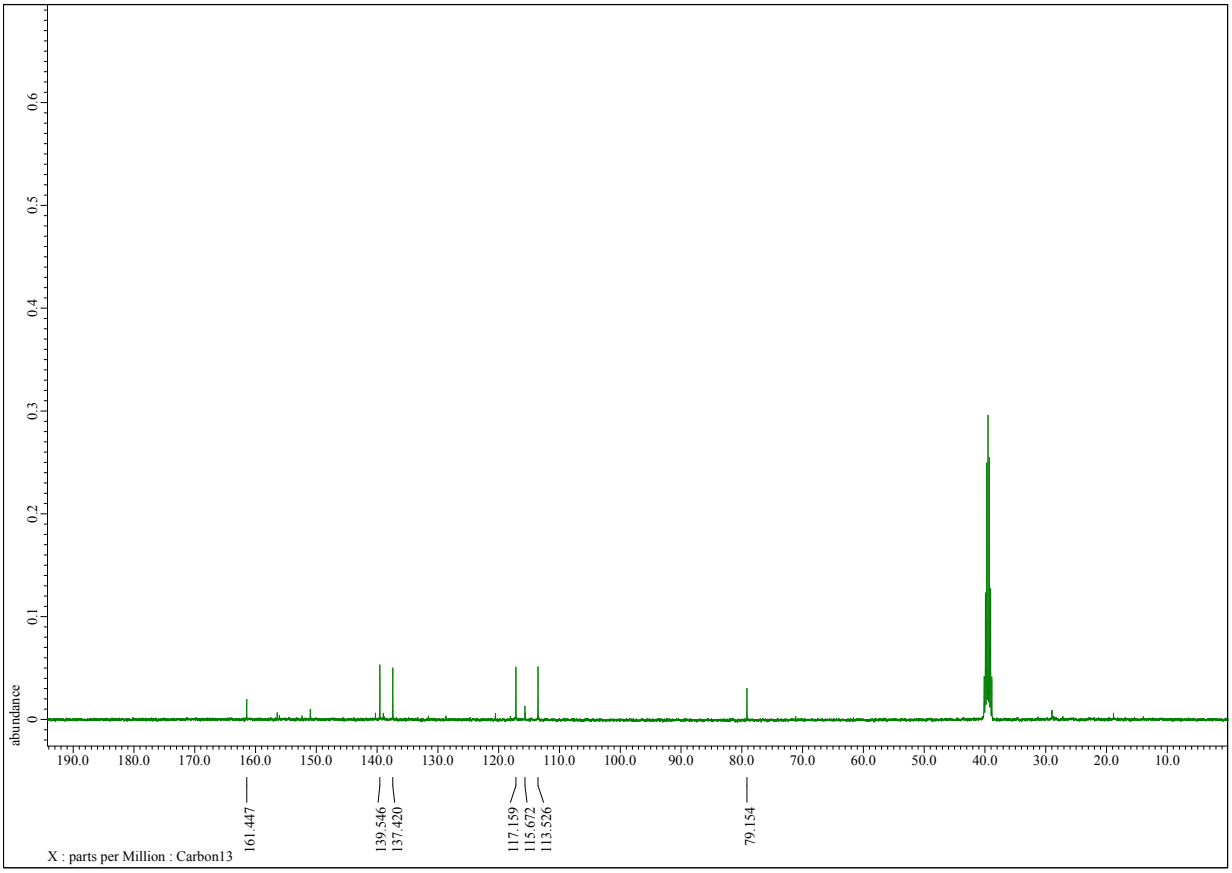

Figure S6. ^{13}C NMR spectrum of **2** in DMSO-d_6.

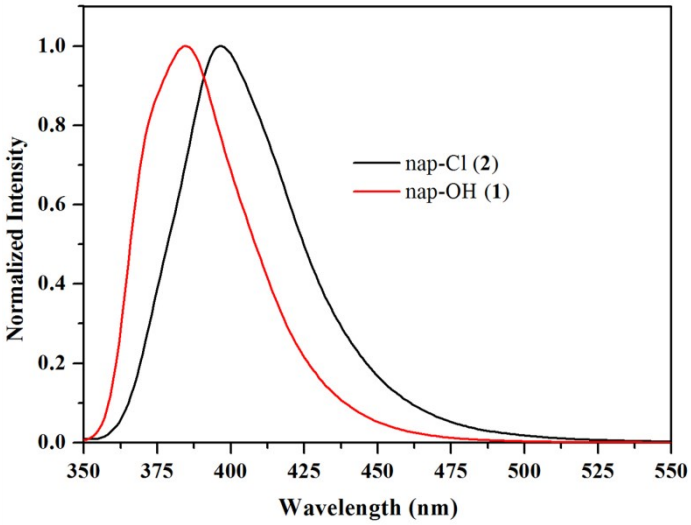

Figure S7. The fluorescence spectra of **1** and **2** in CH_3OH exhibits strong emission at 385 and 397 nm respectively, when excited at 340 and 345 nm.

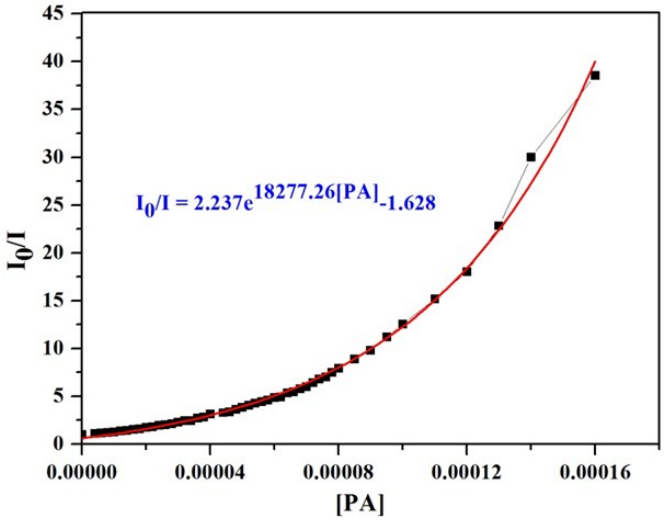

Figure S8. Stern-Volmer plot (I_0/I *versus* [PA]) for sensor **1** in CH_3OH.

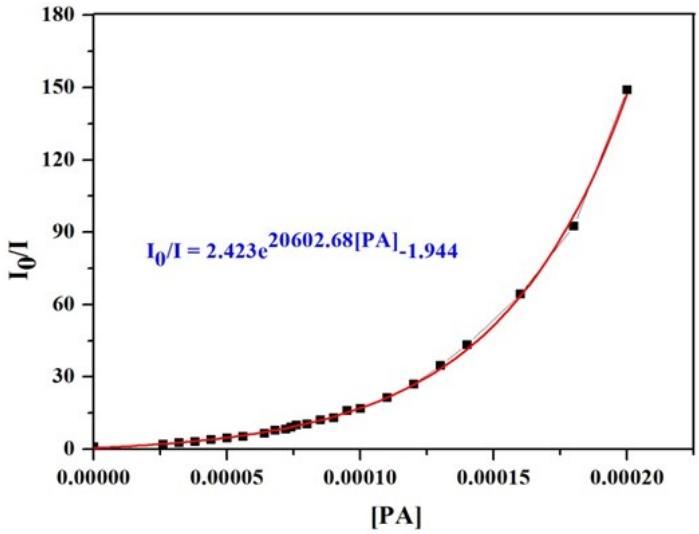

Figure S9. Stern-Volmer plot (I_0/I *versus* [PA]) for sensor **2** in CH_3OH.

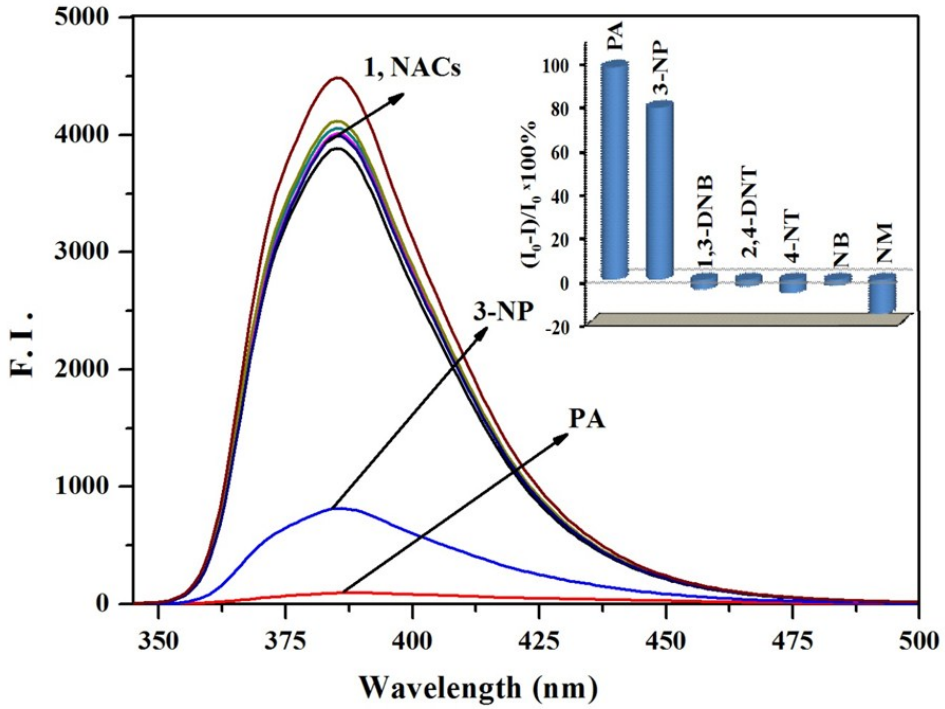

Figure S10. Fluorescence quenching efficiency of **1** in methanol after addition of 4.0 equiv. of each NACs.

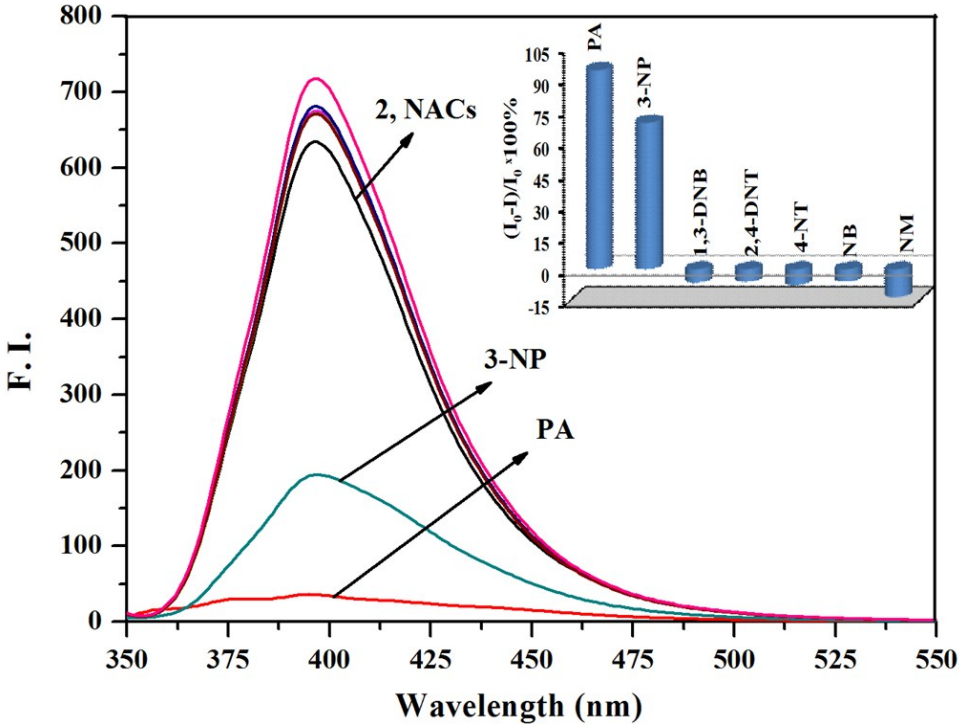

Figure S11. Fluorescence quenching efficiency of **2** in methanol after addition of 4.0 equiv. of each NACs.

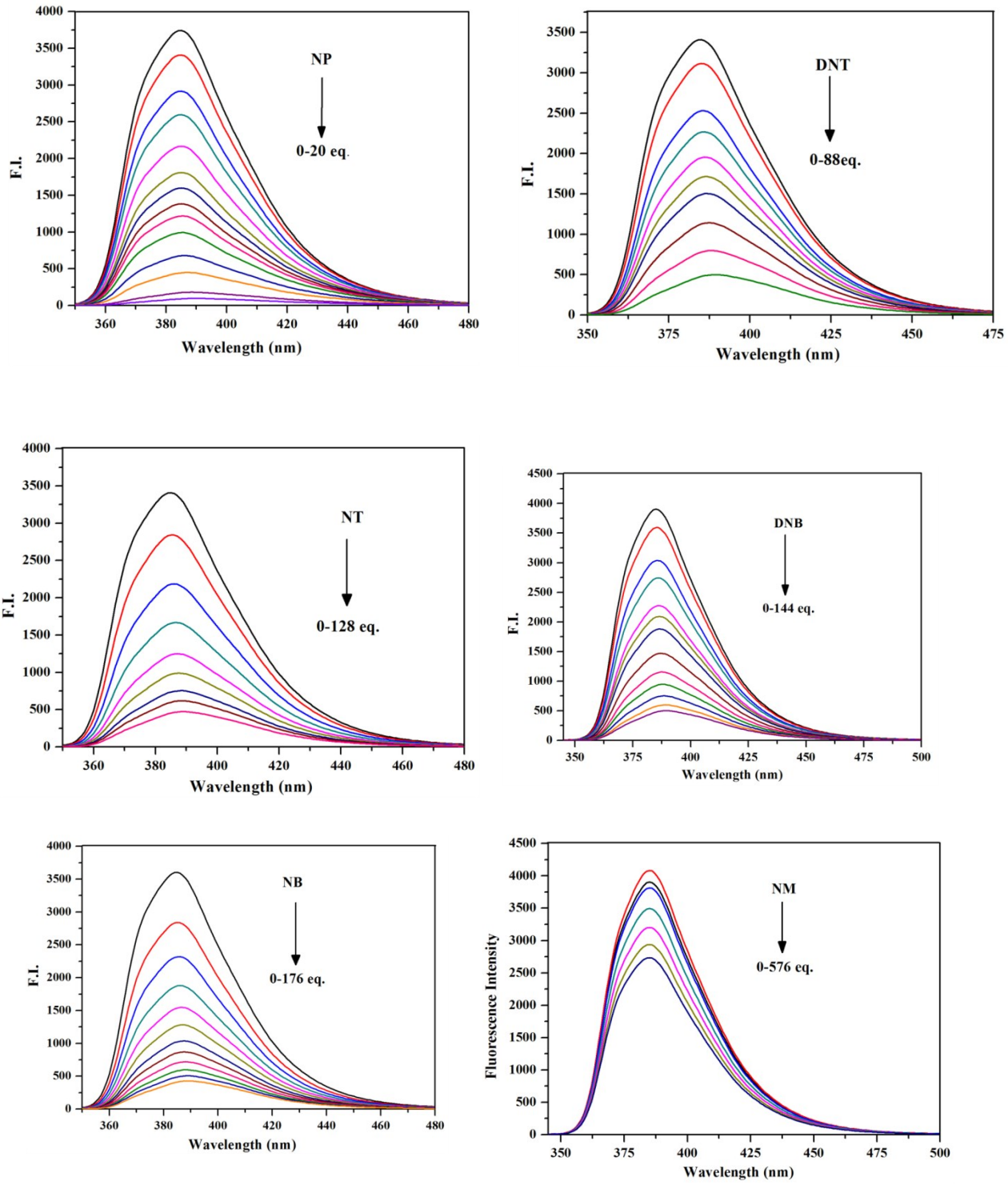

Figure S12. Change in fluorescence spectrum of nap-OH (**1**) (40 μM) upon incremental addition of 3-nitrophenol (NP), dinitrotoluene (DNT), nitrotoluene (NT), dinitrobenzene (DNB), nitrobenzene (NB), nitromethane (NM) in methanol at 298 K.

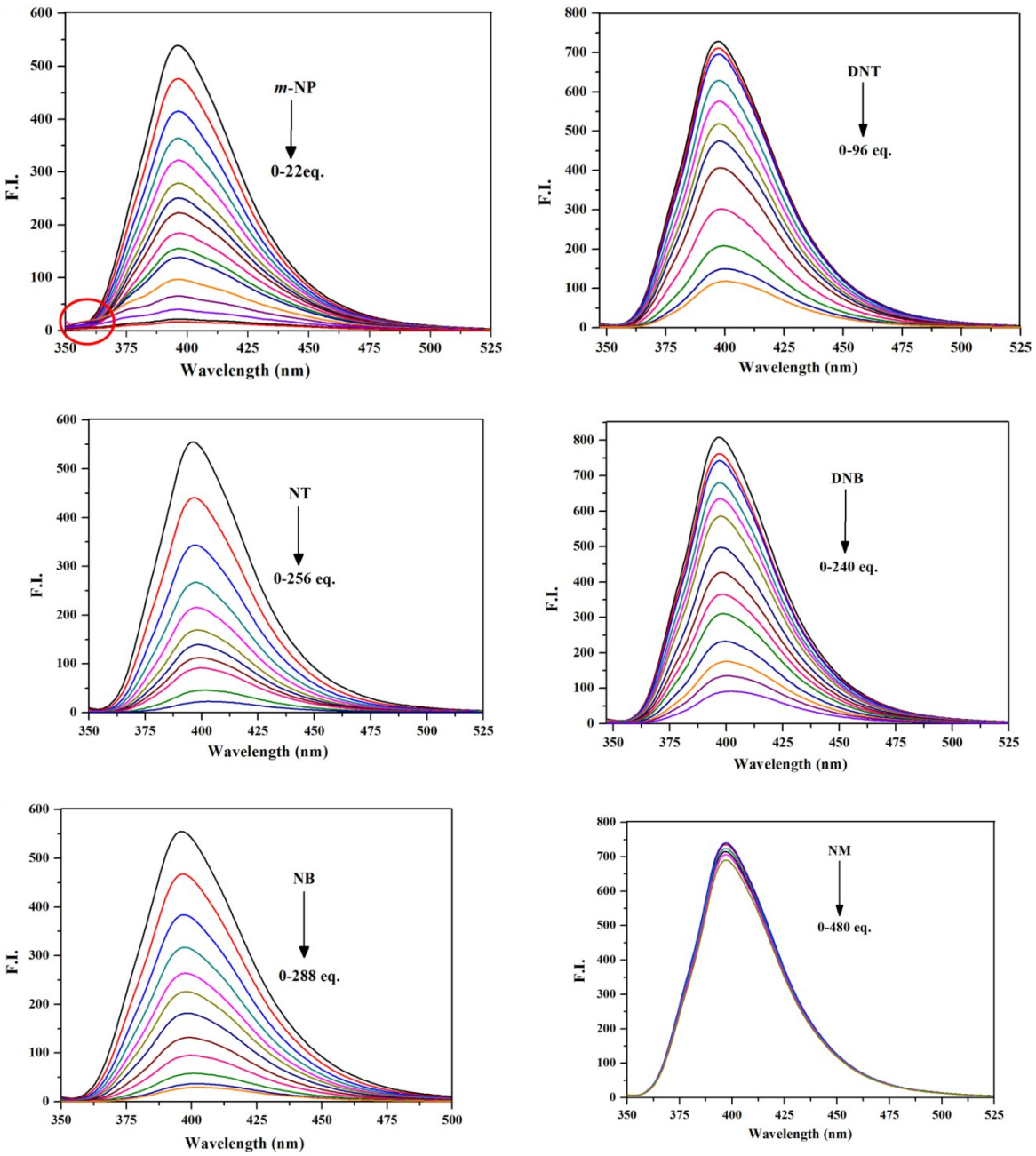

Figure S13. Change in fluorescence spectrum of nap-Cl (**2**) (40 μM) upon incremental addition of 3-nitrophenol (NP), dinitrotoluene (DNT), nitrotoluene (NT), dinitrobenzene (DNB), nitrobenzene (NB), nitromethane (NM) in methanol.

Detection Limit:

The detection limit was calculated from the fluorescence quenching titration experiment. The intercept to X-axis (here log[PA]) was obtained by linear fitting of the $(I_{max}-I)/(I_{max}-I_{min})$ vs log[PA], where I_{max}, I and I_{min} are the initial fluorescence intensity, intensity at particular concentration and intensity at saturation point respectively. Detection limits were calculated by the formula, $([PA] \times MW_{PA})/1000$ (multiplied by 10^6 to get the values in ppm), where MW_{PA} is the molecular weight of PA.[17]

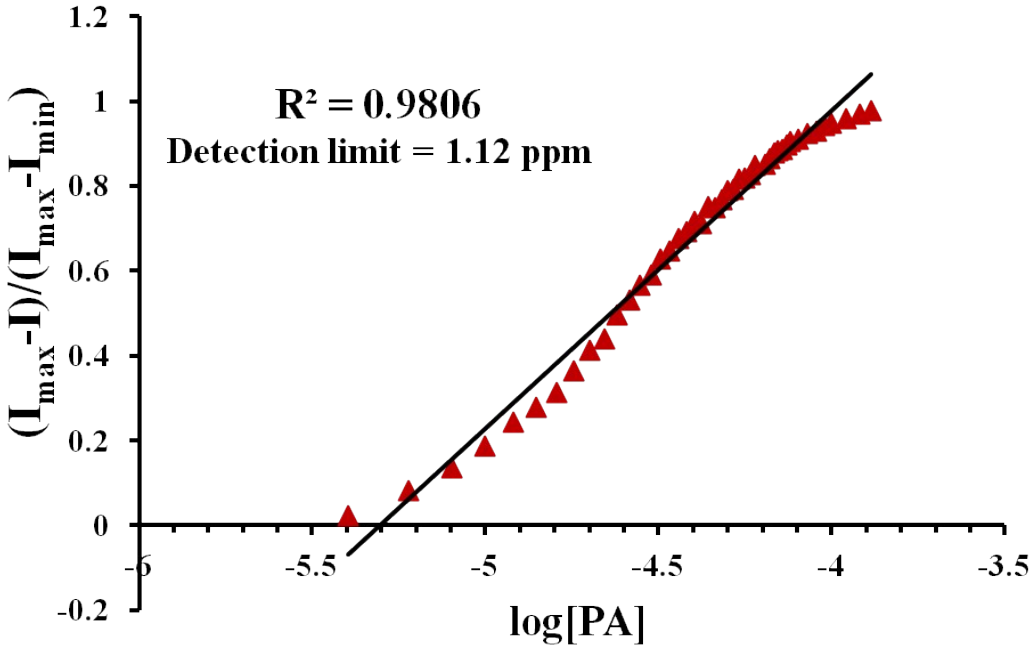

Figure S14. $(I_{max}-I)/(I_{max}-I_{min})$ vs log[PA] plots for **1**. The intercept at X-axis shows the lowest concentrations of PA which can be detected by the sensor.

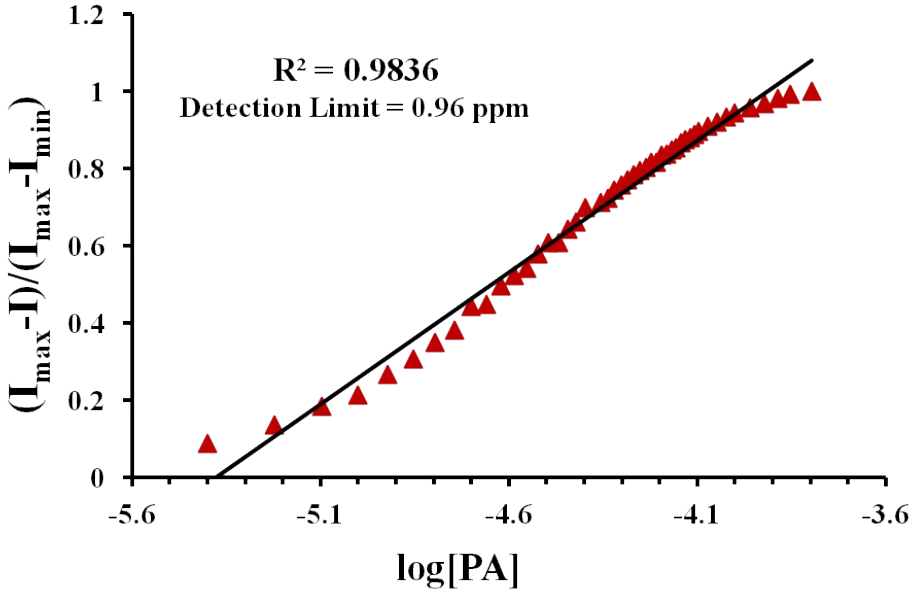

Figure S15. $(I_{max}-I)/(I_{max}-I_{min})$ vs log[PA] plots for **2**. The intercept at x-axis shows the lowest concentrations of PA which can be detected by the sensor.

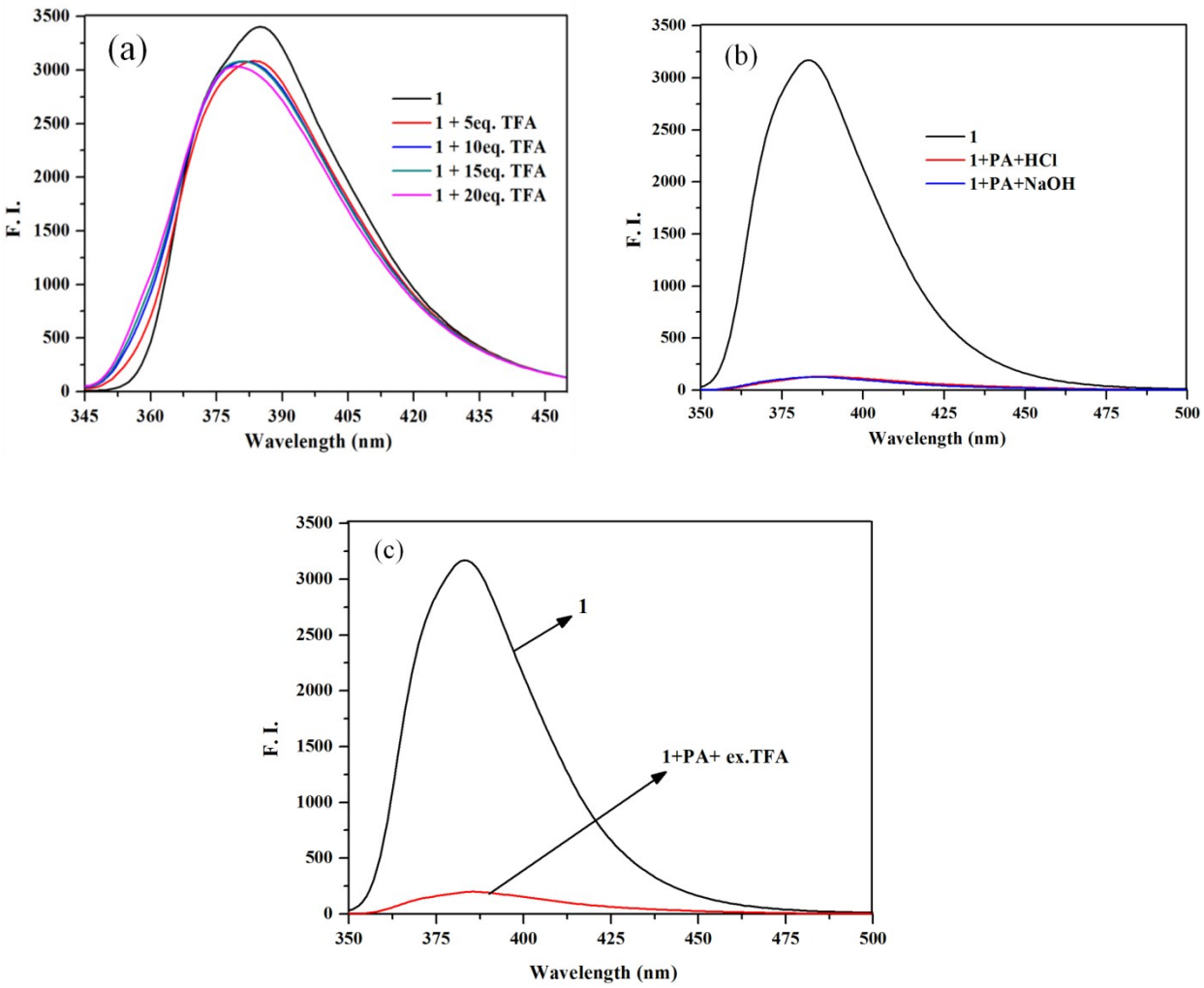

Figure S16. Change in the fluorescence intensity of sensor **1** (a) upon addition of TFA (b) under acidic and basic conditions (c) in the presence of excess TFA in 80% H_2O-CH_3OH.

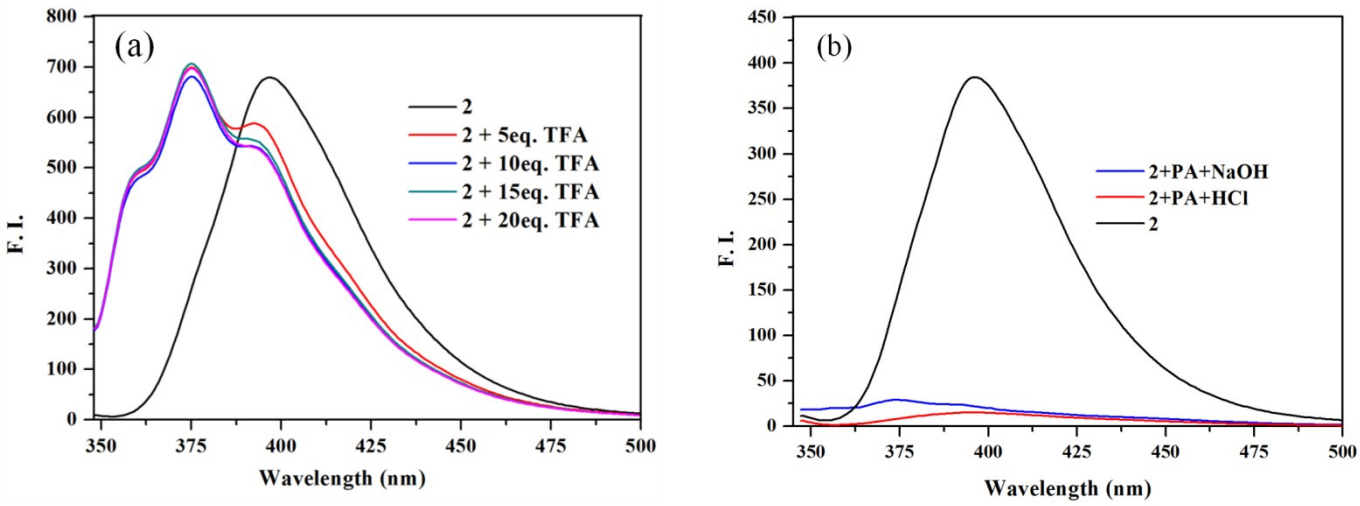

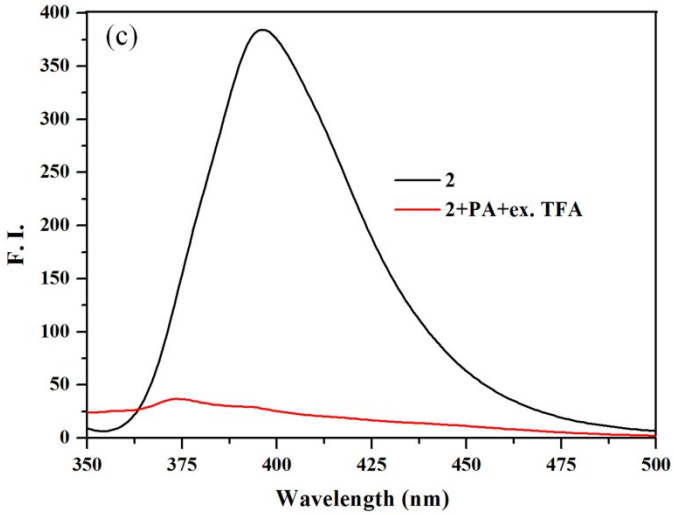

Figure S17. Change in the fluorescence intensity of sensor **2** (a) upon addition of TFA (b) under acidic and basic conditions (c) in the presence of excess TFA in 80% H_2O-CH_3OH.

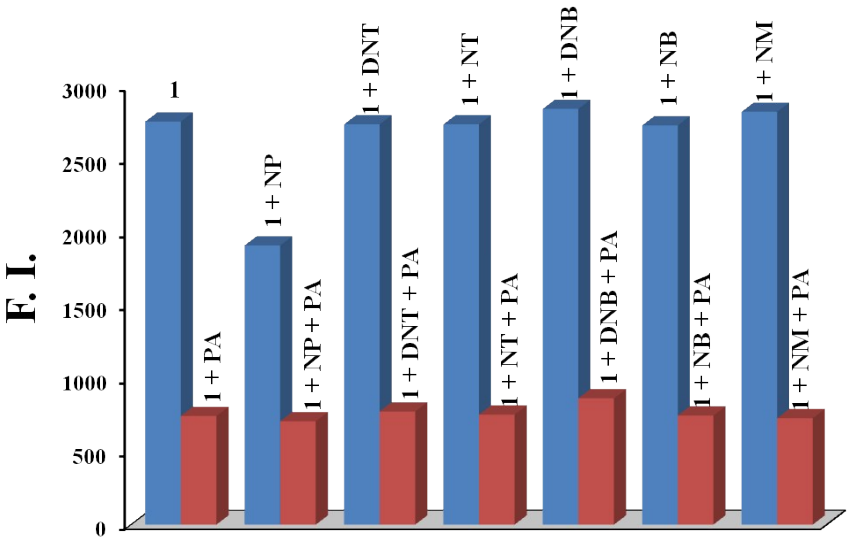

Figure S18. Ratiometric fluorescence changes of **1** on addition of 1 equiv. of PA and 1 equiv. of other NACs. Blue bars indicate the blank and various NACs, and red bars indicate the addition of PA to interfering NACs.

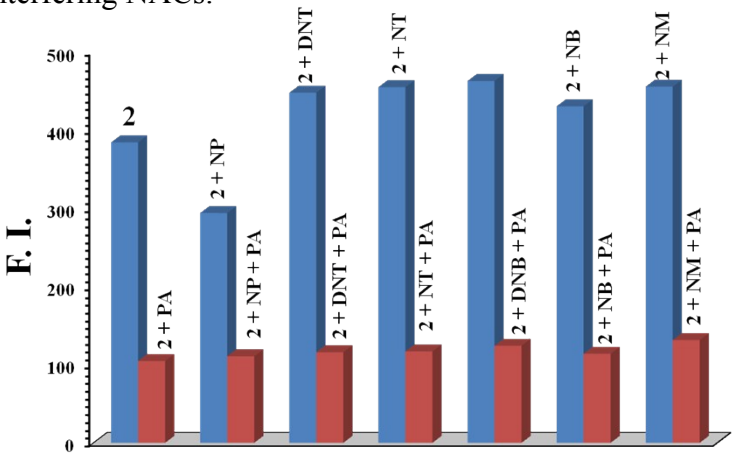

Figure S19. Ratiometric fluorescence changes of **2** on addition of 1 equiv. of PA and 1 equiv. of other NACs. Blue bars indicate the blank and various NACs, and red bars indicate the addition of PA to interfering NACs.

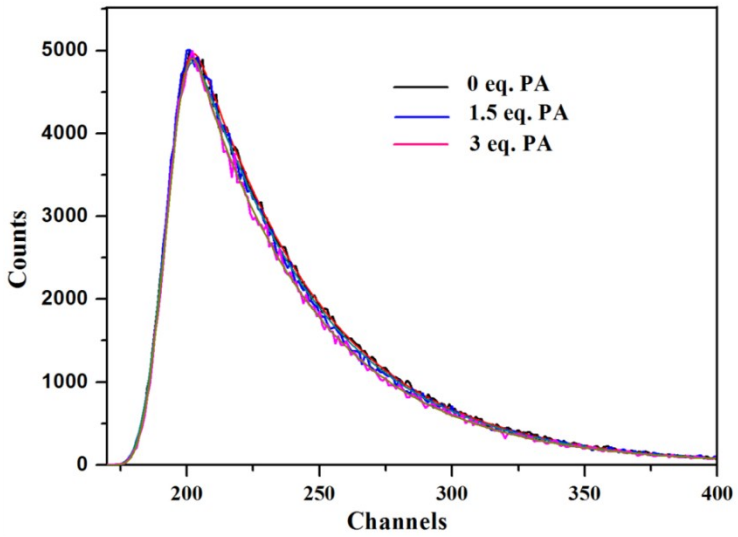

Figure S20. Time-resolved fluorescence decays of nap-OH (**1**) before and after the addition of known concentration of PA. (λ_{ex} = 340nm; λ_{em} = 385 nm).

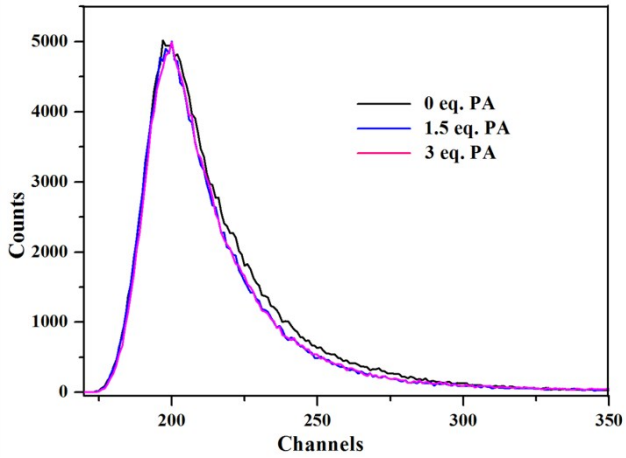

Figure S21. Time-resolved fluorescence decays of nap-Cl (**2**) before and after the addition of known concentration of PA. (λ_{ex} = 345 nm; λ_{em} = 397 nm).

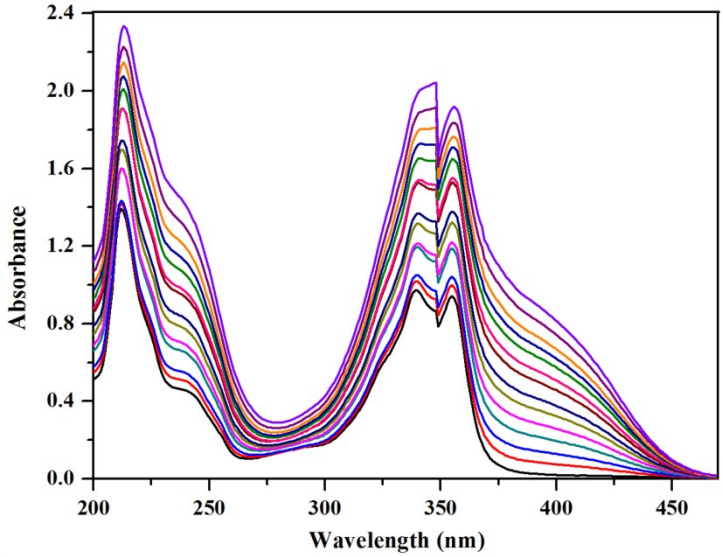

Figure S22. UV-Vis spectral changes of nap-OH (**1**) while increasing [PA] in MeOH.

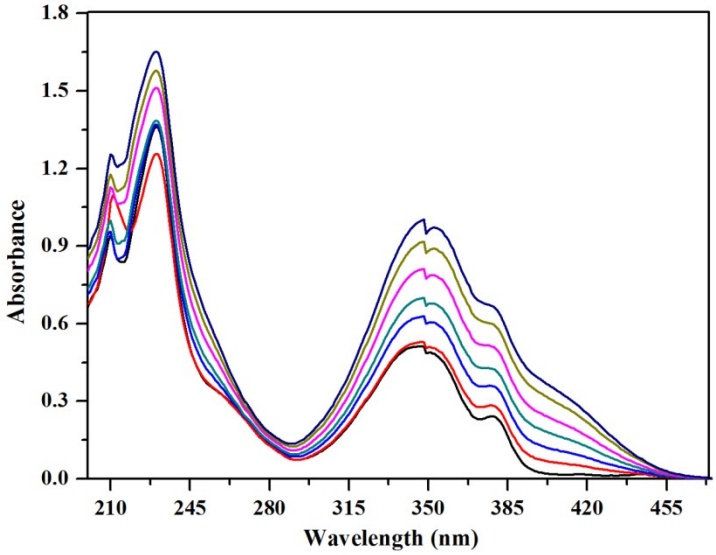

Figure S23. UV-Vis spectral changes of nap-Cl (**2**) while increasing [PA] in MeOH.

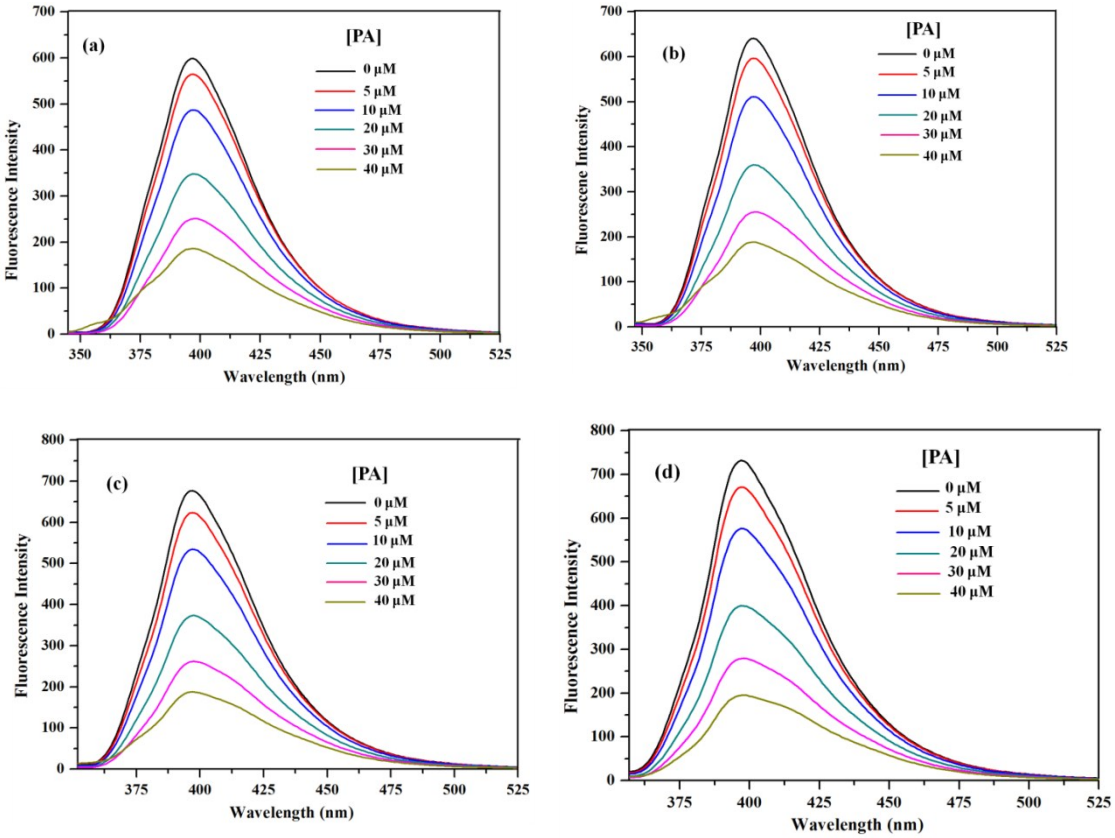

Figure S24. Fluorescence titration of sensor **2** with addition of PA at various excitation wavelengths (a) 340, (b) 345, (c) 350, (d) 360 nm and no significant changes in quenching efficiency of PA were observed.

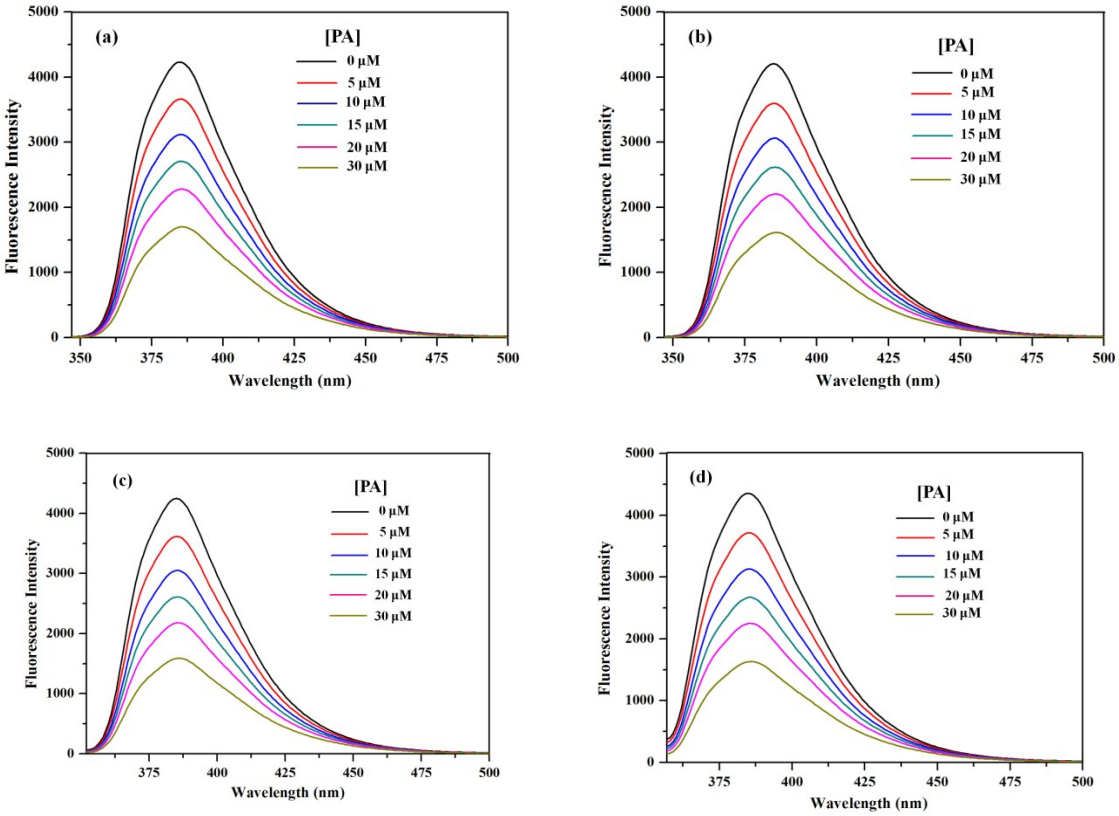

Figure S25. Fluorescence titration of sensor **1** with addition of PA at various excitation wavelengths (a) 340, (b) 345, (c) 350, (d) 360 nm and no significant changes in quenching efficiency of PA were observed.

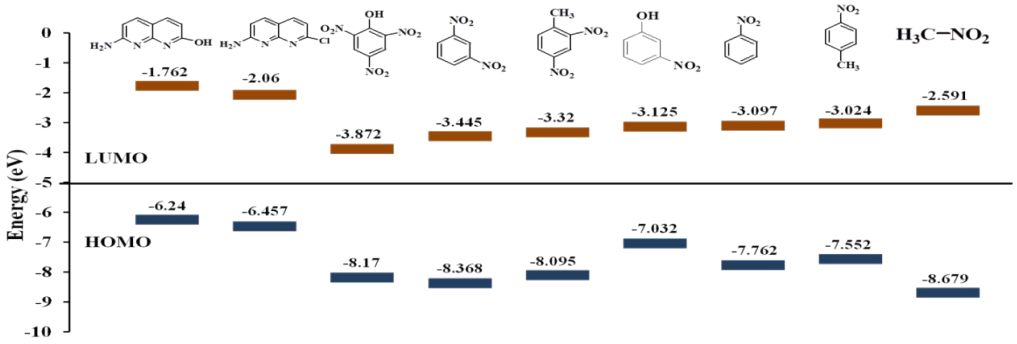

Figure S26. HOMO and LUMO energies of the frontier orbitals of the fluorophores and NACs analytes in methanol.

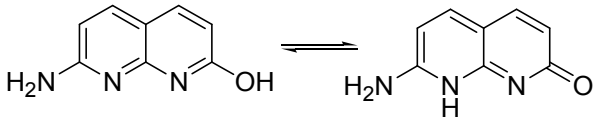

Figure 27. Tautomeric forms of sensor **1**.

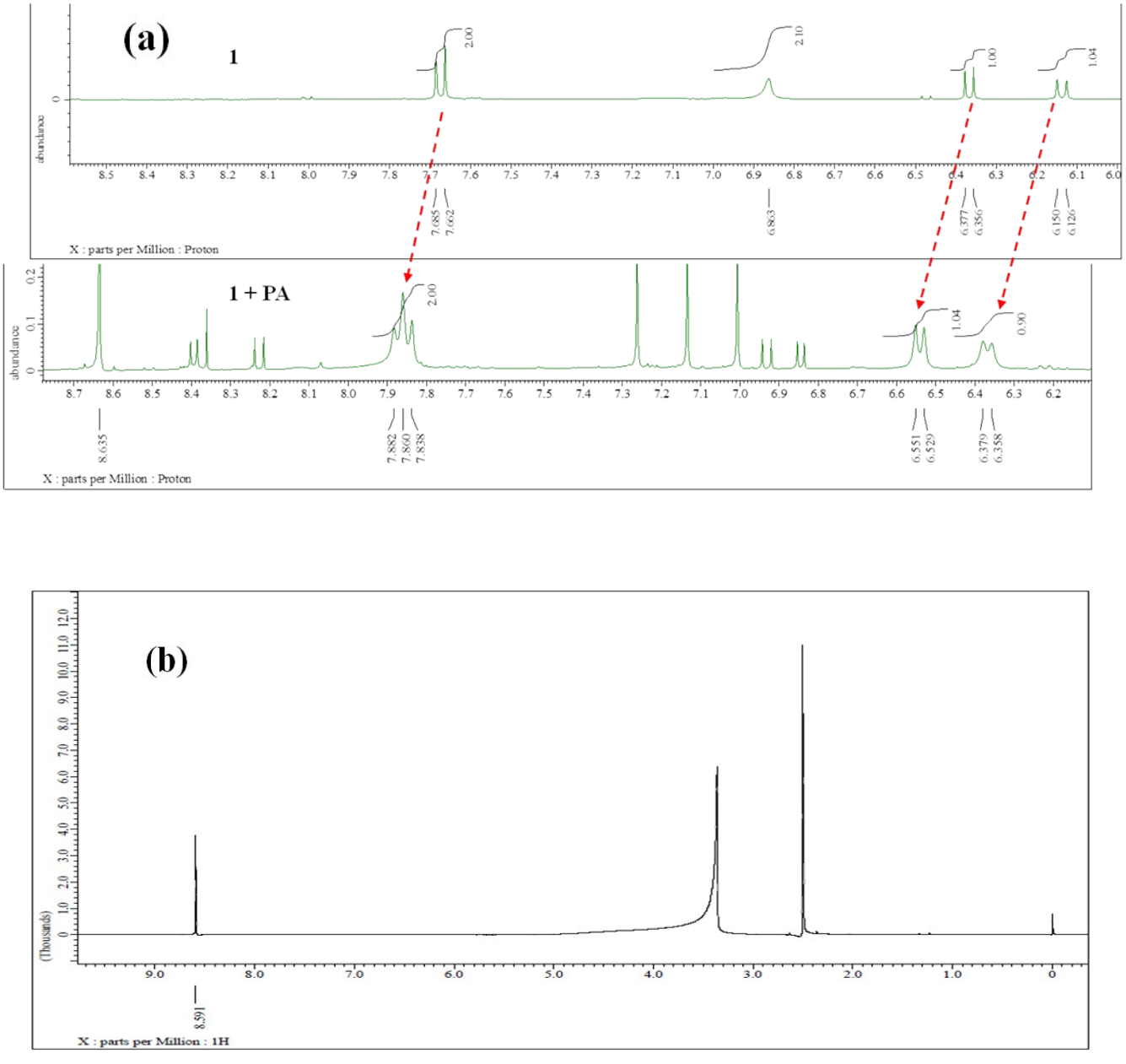

Figure S28. (a) ^{1}H NMR spectra (400 MHz) of the sensor **1** in presence and absence of PA in DMSO-d_6. (b) ^{1}H NMR spectra of PA in DMSO-d_6.

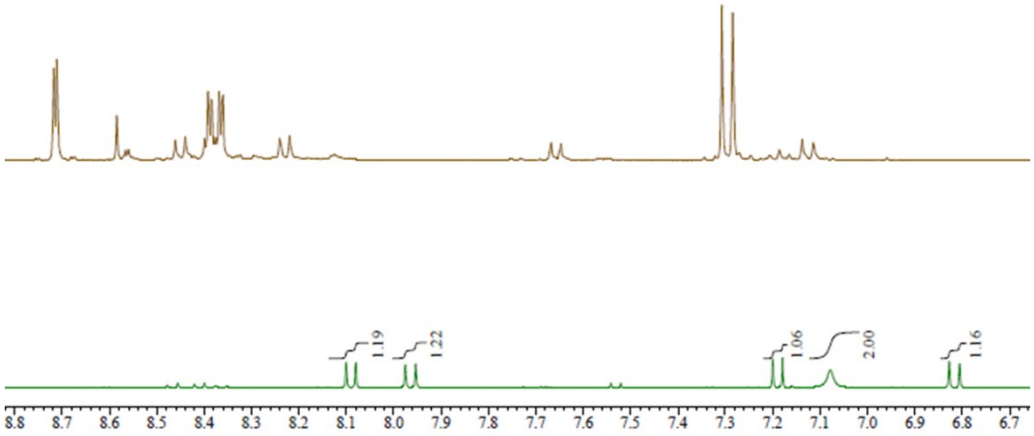

Figure S29. ^{1}H NMR spectra (400 MHz) of the sensor **2** in presence and absence of *m*-nitrophenol in DMSO-d_6.

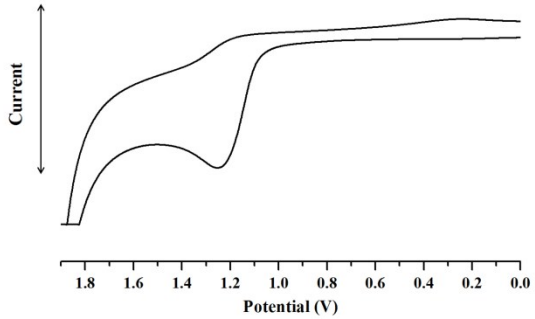

Figure S30. Cyclic voltammogram of nap-OH (**1**).

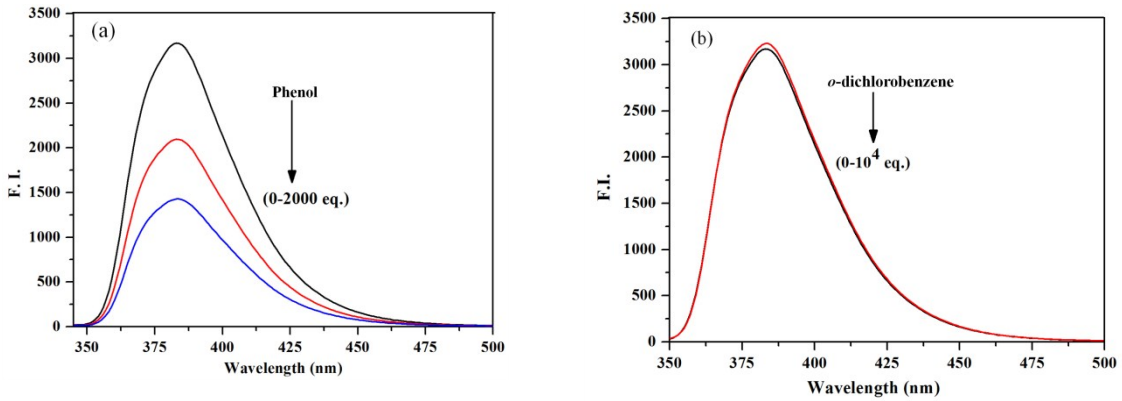

Figure S31. Change in fluorescence spectrum of nap-OH (**1**) (40 μM) upon incremental addition of (a) phenol and (b) o-dichlorobenzene in 80% H_2O-CH_3OH mixture.

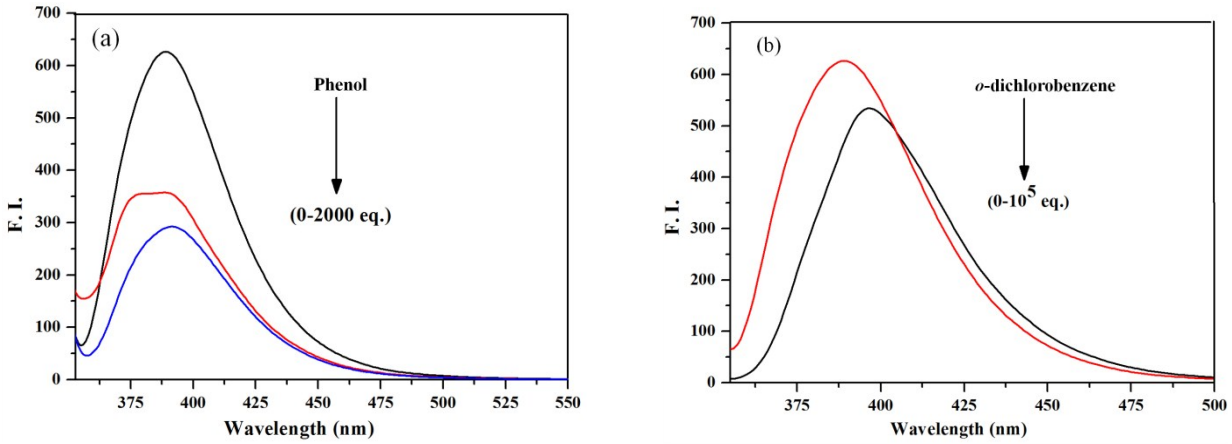

Figure S32. Change in fluorescence spectrum of nap-Cl (**2**) (40 μM) upon incremental addition of (a) phenol and (b) o-dichlorobenzene in 80% H_2O-CH_3OH mixture.

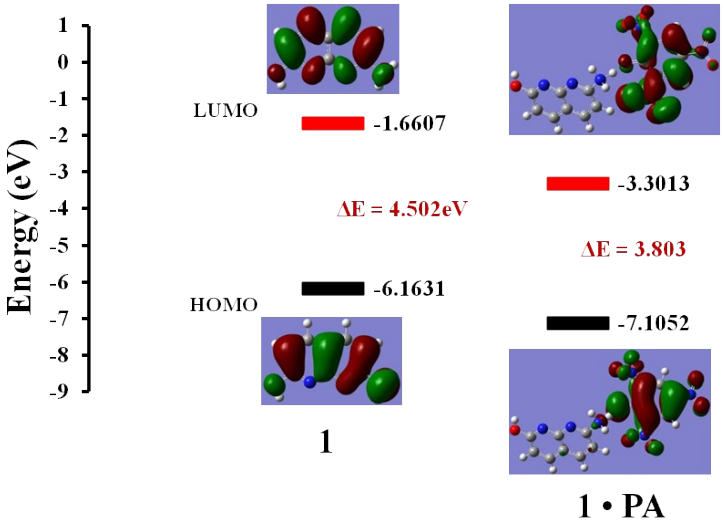

Figure S33. HOMO and LUMO orbital of sensor **1** and **1•PA** calculated by B3LYP method with the 6-311+G(d,p) basis set.

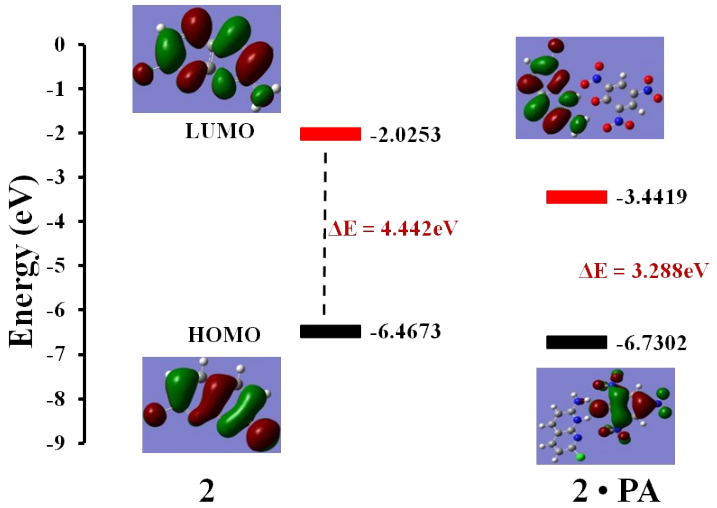

Figure S34. HOMO and LUMO orbital of sensor **2** and **2•PA** calculated by B3LYP method with the 6-311+G(d,p) basis set.

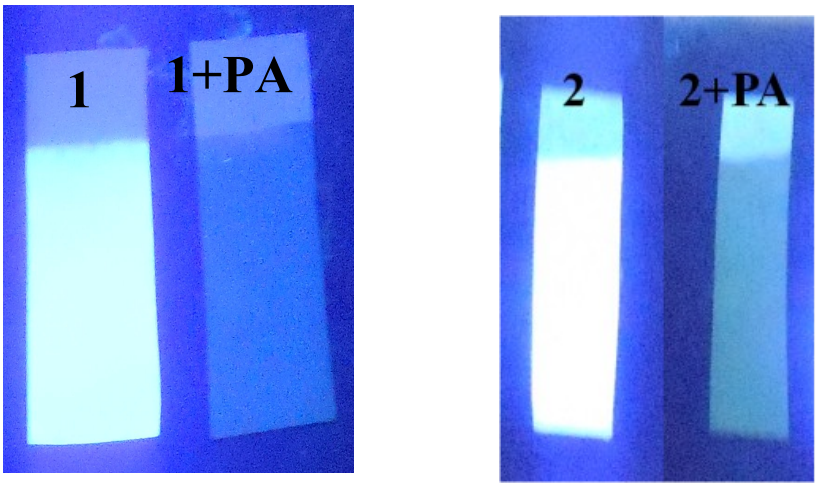

Figure S35. Responses of test strips before and after the addition of picric acid under UV-light.